



Quasiparticle approach to the transport in infinite-layer nickelates

Steffen Bötzel , Ilya M. Eremin , and Frank Lechermann

Institut für Theoretische Physik III, Ruhr-Universität Bochum, D-44780 Bochum, Germany



(Received 13 March 2023; revised 10 May 2023; accepted 16 May 2023; published 30 May 2023)

The normal-state transport properties of superconducting infinite-layer nickelates are investigated within an interacting three-orbital model. It includes effective Ni- d_{z^2} and Ni- $d_{x^2-y^2}$ bands as well as the self-doping band degree of freedom. The thermopower, Hall coefficient, and optical conductivity are modeled within a quasiparticle approximation to the electronic states. Qualitative agreement in comparison to experimentally available Hall data is achieved, with notably a temperature-dependent sign change of the Hall coefficient for larger hole doping x . The Seebeck coefficient changes from negative to positive in a nontrivial way with x , but generally shows only a modest temperature dependence. The optical conductivity shows a pronounced Drude response and a prominent peak structure at higher frequencies due to interband transitions. While the quasiparticle picture is surely approximative to low-valence nickelates, it provides enlightening insights into the multiorbital nature of these challenging systems.

DOI: [10.1103/PhysRevB.107.174526](https://doi.org/10.1103/PhysRevB.107.174526)

I. INTRODUCTION

Thin films of low-valence nickelates in infinite-layer and multilayer form show superconductivity upon hole doping with $T_c \sim 15$ K [1–4]. These long sought-after findings brought new life to the research on superconducting oxides and challenge also the current understanding of high- T_c layered cuprates. In fact, while the superconducting domes with hole doping in these structurally similar nickelates and cuprates resemble each other [2], various normal-state properties apparently differ. For instance, though sizable antiferromagnetic (AFM) correlations are present in infinite-layer nickelates $R\text{NiO}_2$ [5–7], with rare-earth ions $R = \text{La, Pr, Nd}$, the solid stoichiometric AFM order known from cuprates remains elusive.

Furthermore, the transport properties of $R\text{NiO}_2$, with and without hole doping of the form $R_{1-x}\text{Sr}_x\text{NiO}_2$, display remarkable differences to the cuprates ones. At stoichiometry, the (charge-transfer) insulating character of copper oxides is contrasted by weak metallicity in the nickel oxides. This experimental finding of a system in between the metal and insulator has been foreseen by an early quantum-chemistry description by Choynet *et al.* [8]. Later density functional theory (DFT) calculations [9–13] proved the existence of an additional so-called self-doping (SD) band that adds electron pockets to an otherwise Ni- $d_{x^2-y^2}$ dominated Fermi surface in the weakly correlated limit. These electron pockets are the result of hybridization between non- $d_{x^2-y^2}$ Ni($3d$) and $R(5d)$ orbitals. First-principles calculations show that the electron pockets remain at the Fermi level upon including electron correlation beyond DFT. Yet the degree of quasiparticle (QP) character of the original Ni- $d_{x^2-y^2}$ band is a matter of debate from that vantage point [14]. With hole doping x , the resistivity remains sizable in the well-underdoped regime $x < 0.12$ and also in the well-overdoped regime $x > 0.25$. Thus, the charge-carrier transport is not a straightforward metallic one. Although recent improvements in thin-film preparation yield

an increase in conductivity [15], it does not quite match the wide-temperature-range Fermi-liquid signature of overdoped cuprates. Near optimal doping, the normal-state transport is linear in temperature [15], resembling cuprate transport in that regime. Note also that the Hall coefficient in nickelates changes sign from negative to positive in the superconducting doping region [2], a feature which in experimental works is modeled by an effective two-band picture.

Theoretical accounts of hole-doped infinite-layer nickelates do agree on the principle fact that the SD electron pocket around the Γ point in reciprocal space is shifted upwards in energy and away from Fermi level. But the precise doping level x where this happens depends on the specific theoretical method (setting) used. Note that angle-resolved photoemission measurements providing an identification of the near-Fermi-level electronic states are so far lacking. A concrete picture of the low-energy landscape has for now relied solely on theoretical pictures. This especially concerns the relevant Ni($3d$) orbitals upon changing x . Standard DFT and DFT+dynamical mean-field theory (DMFT) assessments mark the sole relevance of the Ni- $d_{x^2-y^2}$ dispersion, possibly with some remaining SD-pocket contribution, as the key to understand the low-lying electronic states [16–22]. Approaches that additionally allow for explicit ligand-based correlations designate the competition between Ni- $d_{x^2-y^2}$ and Ni- d_{z^2} as essential to decipher the low-energy processes [12,23,24]. There are further approaches, e.g., favoring Hund’s physics [25,26] or a description based on Ni- $d_{x^2-y^2}$ and some effective (interstitial) orbital degree of freedom [27–29].

In this paper, we study the transport in the normal state of infinite-layer nickelates based on the theoretical picture of additionally relevant ligand-based correlations. More concretely, we utilize an interacting model Hamiltonian tailored to the low-energy part of a comprehensive first-principles many-body description of stoichiometric and hole-doped NdNiO_2 [23]. The latter is given by a combination of DFT, DMFT

with a Ni-based correlated subspace, and including an explicit Coulomb interaction on oxygen via the self-interaction correction (SIC), the so-called DFT+sicDMFT approach (see Ref. [30] for more details). Within a quasiparticle approximation to the electronic states, we here reveal key features of the doping-dependent thermopower, Hall coefficient, and optical conductivity.

II. THEORETICAL APPROACH

To calculate the transport properties for the normal state of $\text{Nd}_{1-x}\text{Sr}_x\text{NiO}_2$ for different hole dopings we use a three-dimensional low-energy description of the renormalized band structure. In Ref. [23] it is argued that three effective orbitals are sufficient to describe the electronic degrees of freedom near the Fermi level, namely the Ni- d_{z^2} and Ni- $d_{x^2-y^2}$ orbitals as well as an effective orbital giving rise to the SD band. The latter contains weights from Nd($5d$) orbitals at low energy merged with weights from the remaining Ni- t_{2g} , Ni($4s$), and O($2p$) orbitals.

The model Hamiltonian is obtained from maximally localized Wannier [31] downfolding of the DFT band structure to obtain the hopping integrals $t_{ij}^{mm'}$ between the aforementioned orbitals denoted with m, m' and sites i, j . Adding interaction terms, the Hamiltonian reads

$$H = \sum_{i \neq j, mm' \sigma} c_{im\sigma}^\dagger c_{jm'\sigma} + \sum_i (H_i^{\text{int}} + H_i^{\text{orb}}), \quad (1)$$

where σ denotes the spin projection. The part H_i^{int} describes interactions between both Ni- e_g orbitals via a Slater-Kanamori form, whereas the H_i^{orb} term allows for a shift of the SD band, corrects for double-counting terms of the Ni- e_g interaction, and includes crystal-field terms. Different levels of doping are described by fixing the filling, e.g., half filling for stoichiometry. This minimal Hamiltonian is solved at the mean-field level with rotationally invariant slave bosons (RISBs) at the saddle point [32]. For our calculations we use the renormalized quasiparticle Hamiltonian as obtained by RISB and discussed in detail in Ref. [23]. At strong coupling, the model resembles the physics obtained from the more generic DFT+sicDMFT approach to infinite-layer nickelates. The two key features of this physics are the (near) orbital-selective Mott-insulating state of Ni- $d_{x^2-y^2}$ and a doping-dependent shift of the occupied Ni- d_{z^2} dispersion branch in the $k_z = 1/2$ part of the Brillouin zone, starting to cross the Fermi level at $x \sim 0.1$. This shift is a consequence of the renormalized crystal-field splitting mediated by the static part of the RISB self-energy. The linear-in-frequency term of the RISB self-energy enters in the calculations via the quasiparticle (QP) weights $Z_{mm'}$. The QP weight for the Ni- $d_{x^2-y^2}$ orbital remains finite, but is below $Z = 0.2$ for all hole dopings. In the following we will denote the slave-boson renormalized form of the Hamiltonian H as \tilde{H} . The latter Hamiltonian has recently been employed similarly to compute the resonant inelastic x-ray spectroscopy (RIXS) spectrum of spin fluctuations and resulting superconducting instabilities [33]. Here, it will be used to elucidate a minimal and simple perspective on the intriguing transport properties of infinite-layer nickelates.

The Kubo formalism for correlated electrons [34–38] is applied to the renormalized Hamiltonian using the dipole

approximation, so that we compute it in the long-wavelength limit $\mathbf{q} = \mathbf{0}$. Furthermore, vertex corrections are neglected. These approximations lead to the following expression for the real part of the frequency-dependent electric conductivity,

$$\sigma^{\nu\nu}(\omega) = \frac{2e^2\pi}{\hbar\Omega} \int d\omega' \frac{f(\omega') - f(\omega + \omega')}{\omega} \tau^{\nu\nu}(\omega') \quad (2)$$

using

$$\tau^{\nu\nu}(\omega) = \frac{1}{N} \sum_{\mathbf{k}} \text{Tr}[A_{\mathbf{k}}(\omega + \omega') v_{\mathbf{k}}^\nu A_{\mathbf{k}}(\omega') v_{\mathbf{k}}^\nu], \quad (3)$$

where ν is an index for the renormalized band. Here, the trace is performed in orbital space and the sum over the spin indices is assumed. The spectral function is given by

$$A_{\mathbf{k}}^{mm'}(\omega) = -\frac{1}{\pi} Z_{mm'} \text{Im}(\omega - \tilde{H}_{\mathbf{k}} - i\gamma)_{mm'}^{-1}, \quad (4)$$

with γ chosen to be energy independent, corresponding to a dominant elastic scattering rate. The high level of disorder causes a large elastic scattering rate for which the Seebeck and Hall coefficients are insensitive to details of its temperature dependence. This assumption has already been used to account for the Seebeck coefficient in reduced five- and three-layer nickelates [39]. Further, Ω , N , and $f(\omega)$ denote the volume of the unit cell, the number of points in \mathbf{k} space, and the Fermi function, respectively. The components of the Fermi velocities with explicit orbital dependence are given by

$$v_{\mathbf{k}}^{\nu,mm'} = \nabla_{\mathbf{k}} \tilde{H}_{\mathbf{k}}^{mm'} - i(\rho_m^\nu - \rho_{m'}^\nu) \tilde{H}_{\mathbf{k}}^{mm'}. \quad (5)$$

The second term, in which ρ_m^ν is the displacement of the Wannier orbitals with respect to the center of the unit cell, is important for multiatomic unit cells [37].

Applying the limit $\omega \rightarrow 0$ in Eq. (2) yields the dc conductivity

$$\sigma^{\nu\nu} = \lim_{\omega \rightarrow 0} \sigma^{\nu\nu}(\omega) = \frac{2e^2\pi}{\hbar\Omega} \int d\omega' \left(-\frac{df}{d\omega'} \right) \tau^{\nu\nu}(\omega = 0). \quad (6)$$

Analogously, in the same limit the current-heat correlation function reads

$$\alpha^{\nu\nu} = \frac{2e^2\pi}{\hbar\Omega} \int d\omega' \left(-\frac{df}{d\omega'} \right) \omega' \tau^{\nu\nu}(\omega = 0). \quad (7)$$

The ratio of the traces of the current-heat and current-current correlation functions yields the Seebeck coefficient

$$S = -\frac{k_B}{|e|} \frac{\alpha}{\sigma}. \quad (8)$$

The additional ω' in the frequency integral of Eq. (7) weighs contributions from above and below the Fermi surface with opposite sign such that states above (below) lead to negative (positive) contributions to S . For pure elastic scattering, the Seebeck coefficient is thus a measure of particle-hole asymmetry of the electronic dispersion.

Besides the Seebeck coefficient and the frequency-dependent conductivity, we also obtain a simple estimate for the Hall coefficient

$$R_H = \frac{1}{|e|} \frac{\sigma_{xy}^H}{B\sigma_{xx}^2}, \quad (9)$$

where B is the magnetic field pointing along the z direction. Calculating the real part of the Hall conductivity σ_{xy}^H is more intricate than for the diagonal components [40] and performing the required traces in three spatial dimensions is numerically costly. Therefore, to get a first approximation, we neglect interband terms and calculate contributions from the three-band model following Refs. [41,42], i.e.,

$$\sigma_{xy}^H = \frac{2\pi^2 e^3 B}{3\hbar^2 \Omega} \int d\omega \frac{df}{d\omega} \frac{1}{N} \sum_{\mathbf{k}} A_{\mathbf{k}}(\omega)^3 \left(\frac{\partial \epsilon_{\mathbf{k}}}{\partial k_x} \right)^2 \frac{\partial^2 \epsilon_{\mathbf{k}}}{\partial k_y^2}. \quad (10)$$

We have checked for several settings that, by using this approach and using the rigorous treatment in orbital space described above, give similar qualitative results for the Seebeck coefficient despite some minor quantitative differences.

The appropriate convergence of the k integration over the Brillouin zone, for example according in Eq. (3), is ensured by the choice of the k mesh. Explicitly, we have used at least 540^3 points for the Seebeck and at least 600^3 points for $1/8$ of the Brillouin zone for the calculation of the Hall coefficient. For the optical conductivity sufficient convergence is achieved with 120^3 k points. Numerical integration over energies is always done with 100 points. Due to the appearance of $df/d\omega$ in Eqs. (6) and (7), which is strongly peaked at the Fermi energy, an energy cutoff of $\pm 5k_B T$ is used, where $df/d\omega$ drops to less than 3% of its peak value.

Before discussing the results, let us generally remind about the QP approximation taken in this work. For instance, in a recent doping-dependent DFT+*sic*DMFT study [43] it was revealed that especially in the doping region between stoichiometry and the superconducting phase, the electronic spectrum proves to be very incoherent. In other words, well-defined QPs are only expected in certain regions of the infinite-layer nickelate phase diagram. Still, we believe that a QP-based transport description should be performed and weighed as a reference for further studies. In addition, the sole impact of band-dependent features, dressed by proper renormalization from an electron-electron interaction, may be investigated ideally in this limit.

III. RESULTS

In what follows we present the results for the Seebeck coefficient [Fig. 1(a)], the Hall coefficient [Fig. 1(b)], and the optical conductivity (Fig. 2) based on the effective three-band model \tilde{H} calculated for three characteristic hole concentrations $x = 0$, $x = 0.16$, and $x = 0.3$. To better understand the behaviors we also plot the renormalized band structure in Fig. 3.

As seen from Fig. 1(a), the Seebeck coefficient is weakly temperature dependent for all shown dopings, but negative at stoichiometric concentration and positive for $x = 0.16, 0.3$. This evolution is clearly connected to the upwards shift of the Ni- d_{z^2} band from below to above the Fermi level with increasing hole concentration (see Fig. 3 from left to right). At stoichiometry it is not inside the range $\pm 5k_B T$ for temperatures below 300 K [Fig. 3(e)]. Since Ni- $d_{x^2-y^2}$ is quasilocalized and the corresponding QP band very flat, all

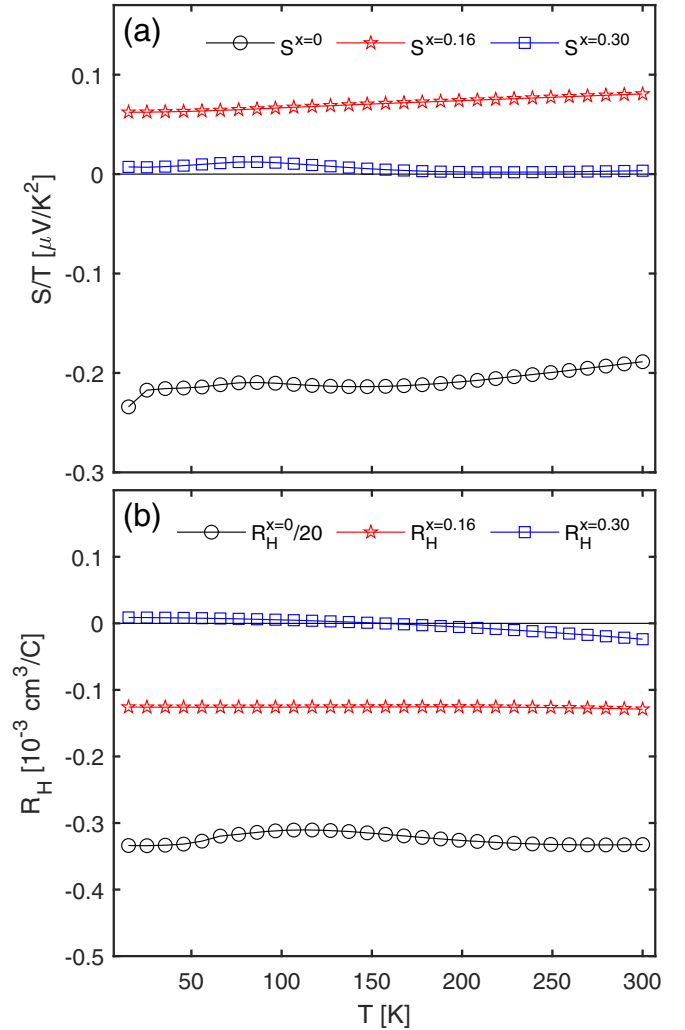


FIG. 1. Calculated temperature dependence of (a) the Seebeck coefficient and (b) the Hall coefficient for various doping concentrations x . Note, the Seebeck coefficient is small but remains positive for $x = 0.3$.

relevant contributions must stem from the SD band, which has an electron character at the Γ point and A point [see Fig. 3(a)].

In the present effective three-band picture, the SD band is also found to be explicitly important for higher dopings. Note also that at $x = 0.06$ the avoided crossing of the SD band and the Ni- d_{z^2} band leads to hole-band-like features directly at the Fermi level around the A point of the Brillouin zone (BZ), as shown in Fig. 3(f). These features would result in a larger and temperature-dependent positive Seebeck coefficient. However, so far it has been difficult to investigate this very low doping range experimentally in great detail, and as mentioned above, it may be that in reality the QP picture breaks down in this region. Because of this uncertainty, we focus here on somewhat higher dopings where the avoided crossings are shifted upwards. For $x = 0.16$ the particle-hole asymmetry of the dispersion at the Fermi level turns out to be positive and shrinking with temperature. For $x = 0.3$ this trend continues and results in tiny but positive values for all temperatures. The upper band is getting close to the

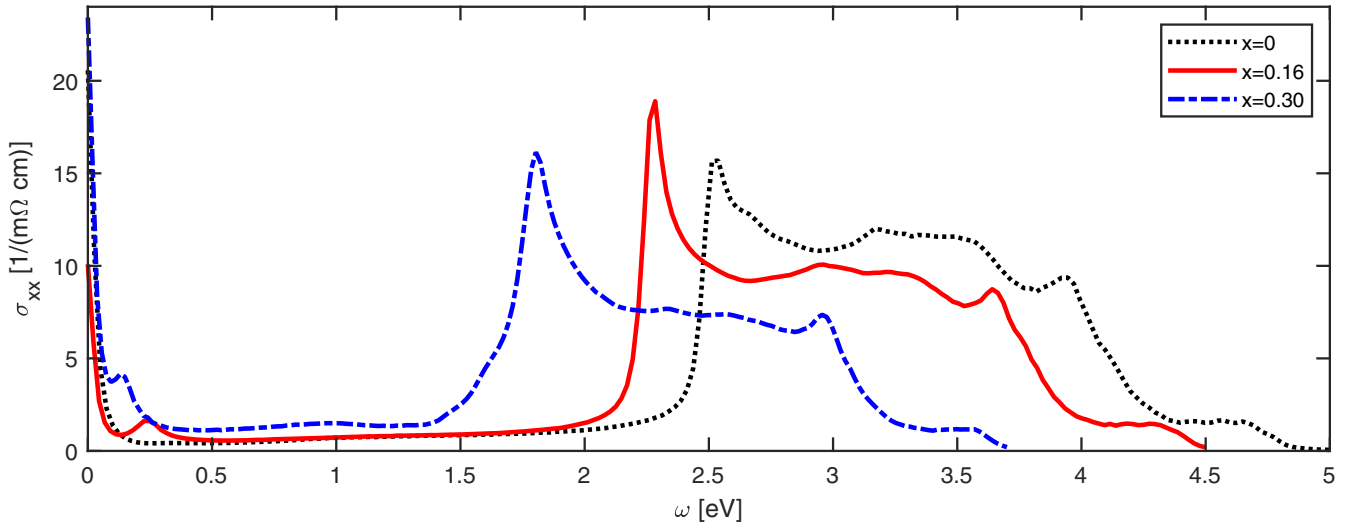


FIG. 2. Calculated optical conductivity for various dopings at a temperature $T = 300$ K.

Fermi surface at Γ and contributes to the thermopower with a negative sign. However, these contributions disappear at about 100 K, where the Seebeck coefficient shows a slight upturn. The rather small magnitude of the thermopower for larger hole dopings is due to a pronounced compensation of electron versus hole carriers. Note that the very flat Ni- $d_{x^2-y^2}$ dispersion with low QP weight yields a negligible contribution for all considered dopings.

Similar to the Seebeck coefficient, the Hall coefficient for the stoichiometric undoped case is determined by the SD electron pockets and therefore negative and much larger than that for the higher hole dopings. Be aware that it is scaled by a factor of 1/20 to properly show it within Fig. 1(b). For dopings $x = 0.16$ and $x = 0.3$ the intriguing interplay between the SD band around A and the relevant quite flat Ni- d_{z^2}

makes the understanding of the definite evolution of the Hall coefficient rather tricky. Correspondingly, the value is much smaller, yet for $x = 0.3$ a robust sign change is revealed at $T \sim 170$ K. This qualitative behavior agrees with experimental Hall data [2,3].

In general, at stoichiometry both the Seebeck and the Hall coefficients display negative and therefore, from an idealistic single-band perspective, dominant electronlike transport. With hole doping this character is initially diminishing in favor of a stronger holelike component. Interestingly, for $x = 0.16$, a weakly holelike Seebeck and weakly electronlike Hall coefficient are revealed, rendering this (superconducting) doping regime of intriguing multiband nature. This is in line with the QP dispersion analysis performed in Ref. [23]. And again, the small Hall coefficient for larger x results from

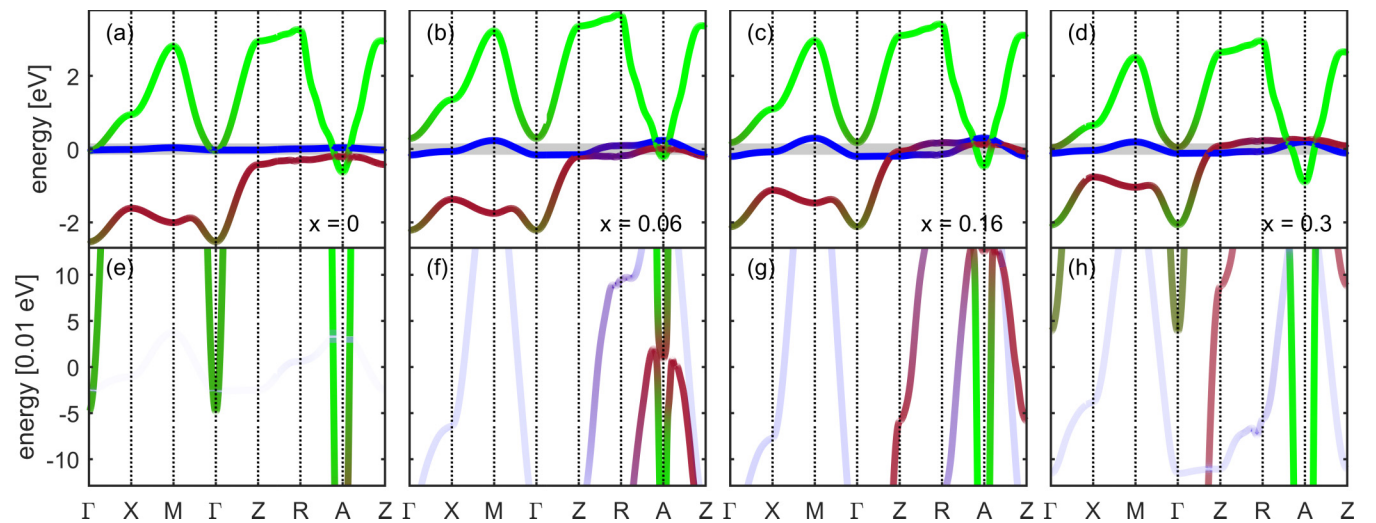


FIG. 3. Calculated renormalized electronic band structure shown along the high-symmetry points Γ - X - M - Γ - Z - R - A - Z . The orbital weights are shown by different colors. In particular, dark red, blue, and green correspond to the Ni- d_{z^2} , Ni- $d_{x^2-y^2}$, and the SD orbital, respectively. The thin gray boxes in (a)–(d) highlight the energy window $5k_B T$ for $T = 300$ K, relevant for the dc conductivity. (e)–(h) show the corresponding zoom in to that energy window. In addition, the shading of the colors follows the QP weight Z of the corresponding bands, shown in the lower panel. This mainly affects the (nearly) half-filled Ni- $d_{x^2-y^2}$ band with small $Z < 0.2$.

nearly compensating electrons and holes. Note that a small thermopower/Hall response may also be realized generally by a strongly enhanced concentration of carriers, which could more directly here relate to the itinerant flat Ni- d_{z^2} band. Such a less pronounced role of the SD pocket at the A point may be more fitting to the full DFT+sicDMFT spectral function with hole doping [43].

The optical conductivity, presented in Fig. 2, is not restricted to contributions from the proximity of the Fermi level and allows therefore deeper insights into the energy dependence of the electronic excitations. In addition to a sharp Drude peak at $\omega = 0$, all the corresponding curves in Fig. 2 show a second peak followed by a plateau towards higher energies. In particular, away from the Drude peak, the Ni- $d_{x^2-y^2}$ band is of negligible importance due to the low quasiparticle weight and the flatness of the band. The peak-plateau feature originates from excitations between Ni- d_{z^2} and SD band. The peak is located at energies slightly higher than the energy difference of the effective bands at the Γ point. In its proximity the dispersions of both bands are similar up to a constant energy shift. This results in good vertical nesting conditions which give rise to that peak. The peak-plateau structure is shifted to lower energies for higher hole dopings x , which is mainly connected to the x -dependent upward shifting of the Ni- d_{z^2} band. At stoichiometry, we find the dc conductivity to be dominated by contributions from the self-doping band. For higher dopings, contributions from the other bands also become important.

Note that in a very first experimental optics study of Nd_{0.8}Sr_{0.2}NiO₂ by Cervasio *et al.*, a sizable Drude peak and not too strong electron correlations were reported in the normal state [44]. This could be in line with the rather itinerant Ni- d_{z^2} band character in this region.

IV. DISCUSSION AND CONCLUSION

Here, we use a realistic low-energy model which is tailored to the strong-coupling regime described by DFT+sicDMFT to study the transport in the infinite-layer nickelates. As discussed in detail in previous works [12,23,43], we believe that this regime is the most promising one to capture the physics of the infinite-layer nickelates. One of the main goals of this work is to study the effects of the predicted Fermi surface crossing of the Ni- d_{z^2} band. We find good qualitative agreement with measured Hall data for stoichiometry and hole dopings $x = 0.16, 0.3$. A temperature-dependent sign change from negative to positive values upon lowering T happens in our modeling at larger x , while the corresponding experimental sign change takes place for $x \sim 0.2$ [2,3]. Agreeing with first experimental suggestions [1] this sign change is due to multiband effects. However, it is not due to a competition between the hole pockets of the Ni- $d_{x^2-y^2}$ band and the electron pockets of the SD band as suggested in Ref. [3]. In our theory, the former band has a negligible contribution because of its flatness and small QP weight. Instead, the Fermi surface is reconstructed as the Ni- d_{z^2} band shifts upwards within the $k_z = 1/2$ plane of the Brillouin zone with doping x . Avoided crossings near the Fermi level result in a more complicated structure in which the SD band is no longer contributing as expected from a straightforward electron pocket. Both the SD

band and Ni- d_{z^2} band and their interplay are thus of importance to obtain the sign change. Note that the sign change of the Hall coefficient has also recently been obtained with a different approach in Ref. [26] for La_{1-x}Sr_xNiO₂. In that work, scattering rates and QP weights are obtained from DMFT and transferred to a two-orbital model. The sign change then results from a coherence-to-incoherence crossover of the Ni- $d_{x^2-y^2}$ states with temperature. However, this crossover is not of strong doping dependence in Ref. [26]. It leads already at stoichiometry to a strong decrease of the absolute value of the Hall coefficient at lower temperature (close to a change of sign), in contrast to experimental data.

To further appreciate the role of the Ni- d_{z^2} band, we showed theoretical results for the Seebeck coefficient. Essentially, we expect it to also change sign from negative to positive with increasing hole doping. In our model this happens due to low-energy band reconstructions as the Ni- d_{z^2} dispersion crosses ϵ_F , whereas contributions of the effectively localized Ni- $d_{x^2-y^2}$ state are again rather small. A recent experimental assessment of the thermopower in the multilayer low-valence nickelates Nd₄Ni₃O₈ and superconducting Nd₆Ni₅O₁₂ by Grissonnanche *et al.* [39] yield a small, nearly T -independent absolute value $< 0.1 \mu\text{V}/\text{K}^2$ and a negative sign for S . These multilayer systems are formally in the well-overdoped region of infinite-layer materials, and thus the small magnitude merged with a weak temperature dependence matches qualitatively with our results. The different sign for this small-magnitude regime may be accidental, however, also note that the low-energy region of the multilayer nickelates with multi-Ni-site unit cells hosts an enlarged complexity compared to the infinite-layer one [45].

To complete the study, we also considered the optical conductivity. A characteristic peak-plateau structure is observed, which is connected to the excitation between the Ni- d_{z^2} band and SD band, which is shifted to lower energies with doping. Comparing the effective QP band structure in Fig. 3 with the more general DFT+sicDMFT spectral function [23], our model clearly does not contain all contributions in the relevant energy range. Note, e.g., that the low-lying Ni- t_{2g} states are excluded in the three-band description. However, the striking features of our model study should still be visible in the full description. For instance, we expect the peak-plateau structure to be visible in optics measurements and observations of its shift to lower energies could provide evidence for the doping-dependent shift of the Ni- d_{z^2} band. Recently [46], the optical conductivity in infinite-layer nickelates has also been studied within a moderate coupling regime based on DFT+DMFT. It is found that within this regime the dc conductivity is too large compared to experiment. This is consistent with our viewpoint, favoring a strong-coupling scenario. However, it is beyond the scope of this work to aim for results beyond the quasiparticle description. A transport investigation based on a comprehensive DFT+sicDMFT study is left for the future.

In conclusion, we here provided a quasiparticle assessment of the transport in infinite-layer nickelates. The qualitative agreement with existing experimental data for the doping-dependent Hall coefficient is encouraging and we look forward to such comparisons between data from our predictions and future transport measurements. As noted, we do not

expect a QP-based description to be fully conclusive for these challenging nickelates, but it serves as an important reference for further investigations of transport in these materials.

ACKNOWLEDGMENT

The work is supported by the German Research Foundation within the bilateral NSFC-DFG Project No. ER 463/14-1.

- [1] D. Li, K. Lee, B. Y. Wang, M. Osada, S. Crossley, H. R. Lee, Y. Cui, Y. Hikita, and H. Hwang, Superconductivity in an infinite-layer nickelate, *Nature (London)* **572**, 624 (2019).
- [2] D. Li, B. Y. Wang, K. Lee, S. P. Harvey, M. Osada, B. H. Goodge, L. F. Kourkoutis, and H. Y. Hwang, Superconducting Dome in $\text{Nd}_{1-x}\text{Sr}_x\text{NiO}_2$ Infinite Layer Films, *Phys. Rev. Lett.* **125**, 027001 (2020).
- [3] S. Zeng, C. S. Tang, X. Yin, C. Li, M. Li, Z. Huang, J. Hu, W. Liu, G. J. Omar, H. Jani, Z. S. Lim, K. Han, D. Wan, P. Yang, S. J. Pennycook, A. T. S. Wee, and A. Ariando, Phase Diagram and Superconducting Dome of Infinite-Layer $\text{Nd}_{1-x}\text{Sr}_x\text{NiO}_2$ thin films, *Phys. Rev. Lett.* **125**, 147003 (2020).
- [4] G. A. Pan, D. F. Segedin, H. LaBollita, Q. Song, E. M. Nica, B. H. Goodge, A. T. Pierce, S. Doyle, S. Novakov, D. C. Carrizales, A. T. N'Diaye, P. Shafer, H. Paik, J. T. Heron, J. A. Mason, A. Yacoby, L. F. Kourkoutis, O. Erten, C. M. Brooks, A. S. Botana *et al.*, Superconductivity in a quintuple-layer square-planar nickelate, *Nat. Mater.* **21**, 160 (2022).
- [5] M. A. Hayward, M. A. Green, M. J. Rosseinsky, and J. Sloan, Sodium hydride as a powerful reducing agent for topotactic oxide deintercalation: synthesis and characterization of the nickel (I) oxide LaNiO_2 , *J. Am. Chem. Soc.* **121**, 8843 (1999).
- [6] H. Lu, M. Rossi, A. Nag, M. Osada, D. F. Li, K. Lee, B. Y. Wang, M. Garcia-Fernandez, S. Agrestini, Z. X. Shen, E. M. Been, B. Moritz, T. P. Devereaux, J. Zaanen, H. Y. Hwang, K.-J. Zhou, and W. S. Lee, Magnetic excitations in infinite-layer nickelates, *Science* **373**, 213 (2021).
- [7] Y. Cui, C. Li, Q. Li, X. Zhu, Z. Hu, Y. Feng Yang, J. Zhang, R. Yu, H.-H. Wen, and W. Yu, NMR evidence of antiferromagnetic spin fluctuations in $\text{Nd}_{0.85}\text{Sr}_{0.15}\text{NiO}_2$, *Chin. Phys. Lett.* **38**, 067401 (2021).
- [8] J. Choisnet, R. A. Evarestov, I. I. Tupitsyn, and V. A. Veryazov, Investigation of the chemical bonding in nickel mixed oxides from electronic structure calculations, *J. Phys. Chem. Solids* **57**, 1839 (1996).
- [9] V. I. Anisimov, D. Bukhvalov, and T. M. Rice, Electronic structure of possible nickelate analogs to the cuprates, *Phys. Rev. B* **59**, 7901 (1999).
- [10] K.-W. Lee and W. E. Pickett, Infinite-layer LaNiO_2 : Ni^{1+} is not Cu^{2+} , *Phys. Rev. B* **70**, 165109 (2004).
- [11] Y. Nomura, M. Hirayama, T. Tadano, Y. Yoshimoto, K. Nakamura, and R. Arita, Formation of 2D single-component correlated electron system and band engineering in the nickelate superconductor NdNiO_2 , *Phys. Rev. B* **100**, 205138 (2019).
- [12] F. Lechermann, Late transition metal oxides with infinite-layer structure: Nickelates versus cuprates, *Phys. Rev. B* **101**, 081110(R) (2020).
- [13] V. Olevano, F. Bernardini, X. Blase, and A. Cano, *Ab initio* many-body *GW* correlations in the electronic structure of LaNiO_2 , *Phys. Rev. B* **101**, 161102(R) (2020).
- [14] H. Chen, A. Hampel, J. Karp, F. Lechermann, and A. Millis, Dynamical mean field studies of infinite layer nickelates: Physics results and methodological implications, *Front. Phys.* **10**, 835942 (2022).
- [15] K. Lee, B. Y. Wang, M. Osada, B. H. Goodge, T. C. Wang, Y. Lee, S. Harvey, W. J. Kim, Y. Yu, C. Murthy, S. Raghu, L. F. Kourkoutis, and H. Y. Hwang, Character of the “normal state” of the nickelate superconductors, [arXiv:2203.02580](https://arxiv.org/abs/2203.02580).
- [16] X. Wu, D. Di Sante, T. Schwemmer, W. Hanke, H. Y. Hwang, S. Raghu, and R. Thomale, Robust $d_{x^2-y^2}$ -wave superconductivity of infinite-layer nickelates, *Phys. Rev. B* **101**, 060504(R) (2020).
- [17] G.-M. Zhang, Y.-F. Yang, and F.-C. Zhang, Self-doped Mott insulator for parent compounds of nickelate superconductors, *Phys. Rev. B* **101**, 020501(R) (2020).
- [18] J. Karp, A. S. Botana, M. R. Norman, H. Park, M. Zingl, and A. Millis, Many-Body Electronic Structure of NdNiO_2 and CaCuO_2 , *Phys. Rev. X* **10**, 021061 (2020).
- [19] I. Leonov, S. L. Skornyakov, and S. Y. Savrasov, Lifshitz transition and frustration of magnetic moments in infinite-layer NdNiO_2 upon hole doping, *Phys. Rev. B* **101**, 241108(R) (2020).
- [20] P. Adhikary, S. Bandyopadhyay, T. Das, I. Dasgupta, and T. Saha-Dasgupta, Orbital-selective superconductivity in a two-band model of infinite-layer nickelates, *Phys. Rev. B* **102**, 100501(R) (2020).
- [21] E. Been, W.-S. Lee, H. Y. Hwang, Y. Cui, J. Zaanen, T. Devereaux, B. Moritz, and C. Jia, Electronic Structure Trends Across the Rare-Earth Series in Superconducting Infinite-Layer Nickelates, *Phys. Rev. X* **11**, 011050 (2021).
- [22] B. Geisler and R. Pentcheva, Correlated interface electron gas in infinite-layer nickelate versus cuprate films on $\text{SrTiO}_3(001)$, *Phys. Rev. Res.* **3**, 013261 (2021).
- [23] F. Lechermann, Multiorbital Processes Rule the $\text{Nd}_{1-x}\text{Sr}_x\text{NiO}_2$ Normal State, *Phys. Rev. X* **10**, 041002 (2020).
- [24] F. Petocchi, V. Christiansson, F. Nilsson, F. Aryasetiawan, and P. Werner, Normal State of $\text{Nd}_{1-x}\text{Sr}_x\text{NiO}_2$ from Self-Consistent *GW* + EDMFT, *Phys. Rev. X* **10**, 041047 (2020).
- [25] P. Werner and S. Hoshino, Nickelate superconductors: Multi-orbital nature and spin freezing, *Phys. Rev. B* **101**, 041104(R) (2020).
- [26] C.-J. Kang and G. Kotliar, Optical Properties of the Infinite-Layer $\text{La}_{1-x}\text{Sr}_x\text{NiO}_2$ and Hidden Hund's Physics, *Phys. Rev. Lett.* **126**, 127401 (2021).
- [27] Y. Gu, S. Zhu, X. Wang, J. Hu, and H. Chen, A substantial hybridization between correlated Ni-d orbital and itinerant electrons in infinite-layer nickelates, *Commun. Phys.* **3**, 84 (2020).
- [28] T. Plienbumrung, M. Daghofer, M. Schmid, and A. M. Oleś, Screening in a two-band model for superconducting infinite-layer nickelate, *Phys. Rev. B* **106**, 134504 (2022).
- [29] M. Jiang, M. Berciu, and G. A. Sawatzky, Stabilization of singlet hole-doped state in infinite-layer nickelate superconductors, *Phys. Rev. B* **106**, 115150 (2022).

- [30] F. Lechermann, W. Körner, D. F. Urban, and C. Elsässer, Interplay of charge-transfer and Mott-Hubbard physics approached by an efficient combination of self-interaction correction and dynamical mean-field theory, *Phys. Rev. B* **100**, 115125 (2019).
- [31] N. Marzari, A. A. Mostofi, J. R. Yates, I. Souza, and D. Vanderbilt, Maximally localized Wannier functions: Theory and applications, *Rev. Mod. Phys.* **84**, 1419 (2012).
- [32] F. Lechermann, A. Georges, G. Kotliar, and O. Parcollet, Rotationally invariant slave-boson formalism and momentum dependence of the quasiparticle weight, *Phys. Rev. B* **76**, 155102 (2007).
- [33] A. Kreisel, B. M. Andersen, A. T. Rømer, I. M. Eremin, and F. Lechermann, Superconducting Instabilities in Strongly Correlated Infinite-Layer Nickelates, *Phys. Rev. Lett.* **129**, 077002 (2022).
- [34] M. Jarrell, J. K. Freericks, and T. Pruschke, Optical conductivity of the infinite-dimensional Hubbard model, *Phys. Rev. B* **51**, 11704 (1995).
- [35] V. S. Oudovenko, G. Pálsson, K. Haule, G. Kotliar, and S. Y. Savrasov, Electronic structure calculations of strongly correlated electron systems by the dynamical mean-field method, *Phys. Rev. B* **73**, 035120 (2006).
- [36] R. Arita, K. Kuroki, K. Held, A. V. Lukoyanov, S. Skornyakov, and V. I. Anisimov, Origin of large thermopower in LiRh_2O_4 : Calculation of the Seebeck coefficient by the combination of local density approximation and dynamical mean-field theory, *Phys. Rev. B* **78**, 115121 (2008).
- [37] J. M. Tomczak and S. Biermann, Optical properties of correlated materials: Generalized Peierls approach and its application to VO_2 , *Phys. Rev. B* **80**, 085117 (2009).
- [38] L. Boehnke and F. Lechermann, Getting back to Na_xCoO_2 : Spectral and thermoelectric properties, *Phys. Status Solidi A* **211**, 1267 (2014).
- [39] G. Grissonnanche, G. A. Pan, H. LaBollita, D. F. Segedin, Q. Song, H. Paik, C. Brooks, A. Botana, J. Mundy, and B. Ramshaw, Seebeck coefficient in a nickelate superconductor: electronic dispersion in the strange metal phase, [arXiv:2210.10987](https://arxiv.org/abs/2210.10987).
- [40] A. A. Markov, G. Rohringer, and A. N. Rubtsov, Robustness of the topological quantization of the Hall conductivity for correlated lattice electrons at finite temperatures, *Phys. Rev. B* **100**, 115102 (2019).
- [41] E. Z. Kuchinskii, N. A. Kuleeva, D. I. Khomskii, and M. V. Sadovskii, Hall effect in doped Mott insulator: DMFT approximation, *JETP Lett.* **115**, 402 (2022).
- [42] P. Voruganti, A. Golubentsev, and S. John, Conductivity and Hall effect in the two-dimensional Hubbard model, *Phys. Rev. B* **45**, 13945 (1992).
- [43] F. Lechermann, Doping-dependent character and possible magnetic ordering of NdNiO_2 , *Phys. Rev. Mater.* **5**, 044803 (2021).
- [44] R. Cervasio, L. Tomarchio, M. Verseils, J.-B. Brubach, S. Macis, S. Zeng, A. Ariando, P. Roy, and S. Lupi, Optical properties of superconducting $\text{Nd}_{0.8}\text{Sr}_{0.2}\text{NiO}_2$ nickelate, [arXiv:2203.16986](https://arxiv.org/abs/2203.16986).
- [45] F. Lechermann, Emergent flat-band physics in $d^{9-\delta}$ multilayer nickelates, *Phys. Rev. B* **105**, 155109 (2022).
- [46] H. LaBollita, A. Hampel, J. Karp, A. S. Botana, and A. J. Millis, Conductivity of infinite-layer NdNiO_2 as a probe of spectator bands, [arXiv:2303.06046](https://arxiv.org/abs/2303.06046).